

Survey Cross-Calibration with *The Cannon*: APOGEE-scale Stellar Labels from LAMOST Spectra

Anna Y. Q. Ho^{1,2}, Melissa K. Ness², David W. Hogg^{2,3,4,5}, Hans-Walter Rix², Chao Liu⁶,
Fan Yang⁶, Yong Zhang⁷, Yonghui Hou⁷, Yuefei Wang⁷

ah@astro.caltech.edu

ABSTRACT

To capitalize on a diverse set of large spectroscopic stellar surveys, it is essential to develop techniques for precise and accurate survey cross-calibration. Here, we demonstrate that this can be achieved by a data-driven approach to spectral modeling: we use *The Cannon* (Ness et al. 2015) to cross-calibrate APOGEE and LAMOST, two large-scale surveys that currently yield inconsistent results due to differing experimental setups and data analysis methodologies. *The Cannon* constructs a predictive model for LAMOST spectra using a reference set of 9952 stars observed in common between the two surveys, taking five labels as ground truth from APOGEE DR12: T_{eff} , $\log g$, $[\text{Fe}/\text{H}]$, $[\alpha/\text{M}]$, and K-band extinction A_{K} . The model is then used to infer T_{eff} , $\log g$, $[\text{Fe}/\text{H}]$, and $[\alpha/\text{M}]$ for 454,180 giant stars in LAMOST DR2, thus tying low-resolution ($R \sim 1800$) LAMOST spectra to the APOGEE ($R \sim 22,500$) label scale. Despite being derived directly from LAMOST spectra, which have lower spectral resolution and very different wavelength coverage, these new Cannon labels have an accuracy and precision comparable to the stated APOGEE DR12 values and uncertainties, essentially eliminating the

¹Cahill Center for Astrophysics, California Institute of Technology, MC 249-17, 1200 E California Blvd, Pasadena, CA, 91125, USA

²Max-Planck-Institut für Astronomie, Königstuhl 17, D-69117 Heidelberg, Germany

³Simons Center for Data Analysis, 160 Fifth Avenue, 7th floor, New York, NY 10010, USA

⁴Center for Cosmology and Particle Physics, Department of Physics, New York University, 4 Washington Pl., room 424, New York, NY, 10003, USA

⁵Center for Data Science, New York University, 726 Broadway, 7th floor, New York, NY 10003, USA

⁶Key Laboratory of Optical Astronomy, National Astronomical Observatories, Chinese Academy of Sciences, Datun Road 20A, Beijing 100012, China

⁷Nanjing Institute of Astronomical Optics & Technology, National Astronomical Observatories, Chinese Academy of Sciences, Nanjing 210042, China

systematic label inconsistencies resulting from the individual survey pipelines. By transferring $[\alpha/M]$ labels from APOGEE, *The Cannon* produces the first $[\alpha/M]$ values measured from LAMOST spectra, and the largest catalog of $[\alpha/M]$ for giant stars to date. This demonstrates that *The Cannon* can successfully bring different surveys onto the same label scale, and effectively transfer label systems from a high-resolution survey to low-resolution spectra.

Subject headings: catalogs — methods: data analysis — methods: statistical — stars: abundances — stars: fundamental parameters — techniques: spectroscopic

1. Survey Cross-Calibration With *The Cannon*

A diverse suite of large-scale spectroscopic stellar surveys (e.g. APOGEE (Majewski et al. 2015), Gaia-ESO (Gilmore et al. 2012), GALAH (De Silva et al. 2015), LAMOST (Zhao et al. 2012), RAVE (Kordopatis et al. 2013), and SEGUE (Yanny et al. 2009)) have been measuring spectra for hundreds of thousands of stars in the Milky Way. They target different types of stars, in different parts of the sky, and at different wavelengths. For example, APOGEE observes in the near-infrared (near-IR) and targets predominantly giants in the dust-obscured mid-plane of the Galaxy, whereas GALAH observes in the optical and targets predominantly nearby main sequence stars. In addition, they observe at different resolutions and employ different data analysis methodologies for using spectra to derive a set of labels characterizing the star, e.g. T_{eff} , $\log g$, $[\alpha/M]$, and $[X/H]$.

These surveys are complementary in their spatial coverage and scientific motivation, and there is enormous scientific promise in combining their results. However, diversity is also the reason why surveys cannot be rigorously stitched together at present: different pipelines measure substantially different labels for the same stars (e.g. Smiljanic et al. (2014)). For example, Chen et al. (2015) compared the three stellar parameters T_{eff} , $\log g$, and $[\text{Fe}/\text{H}]$ between APOGEE and LAMOST, two of the most ambitious ongoing surveys, and found consistency in the photometrically-calibrated T_{eff} but systematic biases in $\log g$ and $[\text{Fe}/\text{H}]$, as Figure 1 shows for 9952 objects observed and analyzed by both surveys.

Although such systematic label offsets may not be surprising for two surveys with disjoint wavelength coverage and very different spectral resolutions (see Section 2), labels are ultimately characteristics of stars and not of observations, and must therefore be unbiased and consistent between surveys to within the stated error bars. To that end, better techniques must be developed for bringing different surveys onto the same label scale.

We approach this cross-calibration problem using *The Cannon* (Ness et al. 2015), a new

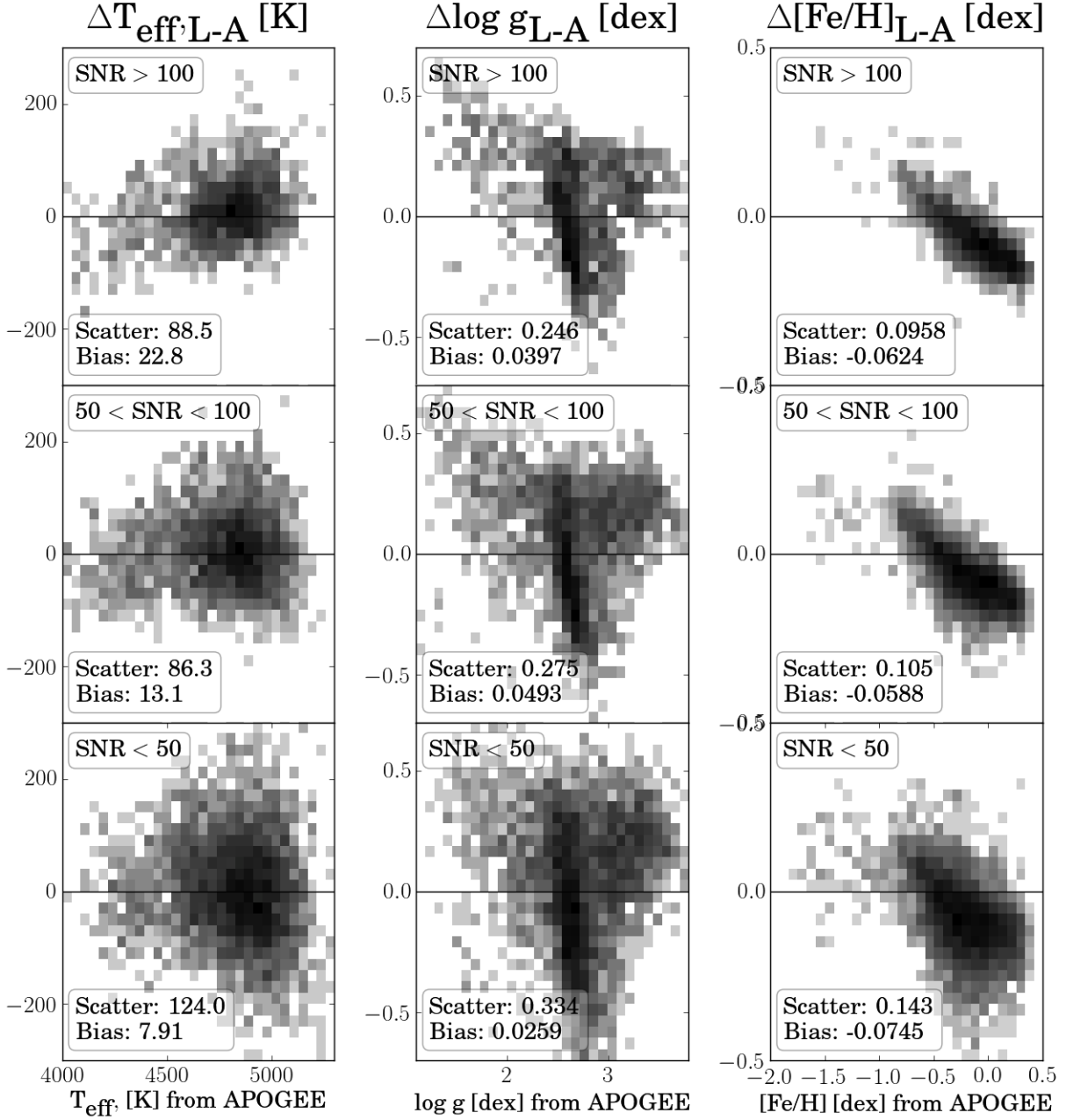


Fig. 1.— Systematic offsets in the labels T_{eff} , $\log g$, and $[\text{Fe}/\text{H}]$ derived by the LAMOST and APOGEE pipelines, for 9952 stars that have been observed and analyzed by both surveys. There are strong biases in $\log g$ and $[\text{Fe}/\text{H}]$. The panel rows show subsets of different LAMOST S/N, calculated for each spectrum by taking the median of the flux-uncertainty ratio across all pixels.

data-driven method for measuring stellar labels from stellar spectra in the context of large spectroscopic surveys. Ness et al. (2015) describe the method and its application to APOGEE DR10 spectra in detail, and Ness et al. (2016) use *The Cannon* and the APOKASC sample to determine masses and ages directly from APOGEE spectra. Here, we recapitulate the fundamental assumptions and steps of *The Cannon* in the context of survey cross-calibration, and describe the procedure more concretely in sections 3 and 4.

Presume that our goal is to cross-calibrate Survey A and Survey B, two spectral surveys that are not (yet) on the same label scale (in other words, the Survey A and Survey B pipelines measure inconsistent labels for objects observed in common, as in Figure 1.) Presume further that we trust Survey A’s labels more than Survey B’s (e.g. because Survey A has higher spectral resolution and higher S/N) and therefore aim to cross-calibrate by bringing Survey B onto Survey A’s label scale.

The Cannon relies on a few key assumptions: that stars with identical labels have very similar spectra, and that spectra vary smoothly with label changes. In other words, the continuum-normalized flux at each pixel in a spectrum is a smooth function of the labels that describe the object. The function that takes the labels and predicts the flux at each wavelength of the spectrum is called the “spectral model”; fitting for the coefficients of the spectral model is the goal of the first step, the “training” step.

In the training step, *The Cannon* uses the objects with spectra from Survey B and labels from Survey A as “reference objects” to fit for the spectral model coefficients at each pixel of the spectrum independently. The spectral model characterizes the flux at each pixel of a Survey B spectrum as a function of corresponding Survey A labels, and predicts what the spectrum of an object observed in Survey B would look like given a set of labels from Survey A.

In the second step, the “test” step, this model is used to derive likely labels for any (similar) object given its spectrum from Survey B, including those not observed by Survey A. Note that if the Survey A pipeline has measured a dozen labels precisely and the Survey B pipeline has only measured three, we can in principle use our model to infer extra, previously unknown labels from Survey B spectra; we dub this process of transferring knowledge of labels from one survey to another “label transfer.” Note also that in this approach, Survey A enters only through its labels, not the data (spectra, light curves, or otherwise) from which these labels were derived, and Survey B enters only through its spectra.

In this work, we take APOGEE to be Survey A and LAMOST to be Survey B. We select APOGEE as the source of the trusted stellar labels because it is the higher-resolution survey ($R \approx 22,500$ versus $R \approx 1,800$ for LAMOST). We use five post-calibrated labels from

APOGEE DR12: T_{eff} , $\log g$, $[\text{Fe}/\text{H}]$, $[\alpha/\text{M}]$, and K-band extinction A_k . While A_k is not strictly an intrinsic property of the stars, it is a “label”, in the sense that it is an immutable property of the stellar spectrum when observed from our location in the Galaxy. We decided to include extinction in constructing the model because the objects in the reference set (in the Galactic mid-plane) include visual extinctions up to $A_v \approx 3.5$ ($A_k \approx 0.4$). This impacts some of the optical spectra in the training step and in the test step, not only by reddening, but also by dust and gas absorption features.

Note that what we call $[\text{Fe}/\text{H}]$ in this work is stored under the header `PARAM_M_H` in DR12. We use this value so that all four labels have gone through the same post-calibration procedure, but refer to it as $[\text{Fe}/\text{H}]$ rather than $[\text{M}/\text{H}]$ because it has been calibrated to the $[\text{Fe}/\text{H}]$ of star clusters (Mészáros et al. 2013), and in order to be consistent with the terminology from LAMOST.

The 11,057 objects measured in common between APOGEE and LAMOST constitute the possible reference set for the training step; in practice, we use 9952 of these objects to fit for the spectral model, then apply this model to infer both new labels for the reference set, as well as labels for the remaining 444,228 LAMOST giants in DR2 *not* observed by APOGEE. By construction, these labels are tied to the APOGEE scale.

This work and Ness et al. (2015) share the same general procedure. The fact that it performs well for spectra at very different wavelength regimes and resolutions illustrates the general applicability of this procedure to large uniform sets of stellar spectra, given a suitable reference set. The methodology is described in detail in Ness et al. (2015) and the procedure here is simply an implementation; the primary distinguishing feature in how the LAMOST spectra were prepared for *The Cannon*, and we describe that process in Section 2.1.

2. Data: LAMOST Spectra and APOGEE Labels

The Large sky Area Multi-Object Spectroscopic Telescope (LAMOST) is a low-resolution ($R \approx 1,800$) optical (3650 – 9000 Å) spectroscopic survey. As of the second data release (DR2; Luo A.L., Bai Z.R. et al. (2015)), LAMOST has obtained spectra for over 4.1 million objects and measured three stellar labels (T_{eff} , $\log g$, $[\text{Fe}/\text{H}]$) for ~ 2.2 million stars. Although the survey does not select for a particular stellar type, many of the stars are red giants; the population of K giants numbers 300,000 in DR1 and 500,000 in DR2 (Liu et al. 2014). Moreover, $> 100,000$ red clump candidates have been identified in the DR2 catalog (Wan et al. 2015). Stellar labels for the LAMOST spectra are derived by the package *ULySS* (Wu et al. 2011), which fits each spectrum to a model spectrum that is a linear combination

of non-linear components, optically convolved with a line-of-sight velocity distribution and multiplied by a polynomial function. Improved surface gravity values have been obtained for the metal-rich giant stars via cross-calibration with asteroseismically-derived values from *Kepler* (Liu et al. 2015).

APOGEE is a high-resolution ($R \approx 22,500$), high-S/N ($S/N \approx 100$), H-band (15200-16900 Å) spectroscopic survey, part of the Sloan Digital Sky Survey III (Majewski et al. (2015); Eisenstein et al. (2011)). Observations are conducted using a 300-fiber spectrograph (Wilson et al. 2010) on the 2.5 m Sloan Telescope (Gunn et al. 2006) at the Apache Point Observatory (APO) in Sunspot, New Mexico (USA) and consist primarily of red giants in the Milky Way bulge, disk, and halo. The most recent data release, DR12 (Alam et al. 2015; Holtzman et al. 2015), comprises spectra for $> 100,000$ red giant stars together with their basic stellar parameters and 15 chemical abundances. The parameters and abundances are derived by the ASPCAP pipeline, which is based on chi-squared fitting of the data to 1D LTE models for seven labels: T_{eff} , $\log g$, $[\text{Fe}/\text{H}]$, $[\alpha/\text{M}]$, $[\text{C}/\text{M}]$, $[\text{N}/\text{M}]$, and micro-turbulence (García Pérez et al. 2015).

2.1. Preparing LAMOST Spectra for *The Cannon*

To be used by *The Cannon*, any spectroscopic data set must satisfy the conditions laid out in Ness et al. (2015). The spectra must share a common line-spread function, be shifted to the rest-frame and sampled onto a common wavelength grid with uniform start and end wavelengths. The flux at each pixel of each spectrum must be accompanied by a flux variance that takes error sources such as photon noise and poor sky subtraction into account; bad data (e.g. regions with skylines and telluric regions) must be assigned inverse variances of zero or very close to zero. Finally, the spectra do not need to be continuum normalized, but they must be normalized in a consistent way that is independent of S/N; more precisely, the normalization procedure should be a linear operation on the data, so that it is unbiased as (symmetric) noise grows.

Preparatory steps were necessary to make the raw LAMOST spectra satisfy these criteria. First, the displacement from the rest-frame was calculated for each spectrum using the redshift value provided in the data file header, and the spectra shifted accordingly. (The redshift values are derived within the LAMOST data pipeline, from their cross-correlation procedure.) Spectra were then re-sampled onto the original grid using linear interpolation. After shifting, we applied lower and upper wavelength cuts and sampled all spectra onto a common wavelength grid spanning 3905 Å – 9000 Å. All of these operations were performed on both the flux and inverse variance arrays.

Each spectrum was normalized by dividing the flux at each λ_0 by $\bar{f}(\lambda_0)$, which was derived by an error-weighted, broad Gaussian smoothing:

$$\bar{f}(\lambda_0) = \frac{\sum_i (f_i \sigma_i^{-2} w_i(\lambda_0))}{\sum_i (\sigma_i^{-2} w_i(\lambda_0))}, \quad (1)$$

where f_i is the flux at pixel i , σ_i is the uncertainty at pixel i , and the weight $w_i(\lambda_0)$ is drawn from a Gaussian

$$w_i(\lambda_0) = e^{-\frac{(\lambda_0 - \lambda_i)^2}{L^2}}, \quad (2)$$

L was chosen to be 50 \AA , much broader than typical atomic lines.

To emphasize, this “normalization” is in no sense “continuum normalization,” and is different from the standard normalization used in spectral analysis. Our goal in preparing the spectra in this way is to simplify the modeling procedure by removing overall flux, flux calibration, and large-scale shape changes from the spectra.

The procedure is illustrated in Figure 2, which shows three spectra corresponding to a sample reference object: its APOGEE spectrum, its LAMOST spectrum overlaid with its Gaussian-smoothed “continuum,” and final “normalized” LAMOST spectrum.

3. The Cannon Training Step: Modeling LAMOST Spectra as a Function of APOGEE Labels

Our reference set comprises 9952 of the 11,057 objects measured in common between LAMOST DR2 and APOGEE DR12. We eliminate stars with unreliable T_{eff} , $\log g$, $[\text{Fe}/\text{H}]$, $[\alpha/\text{M}]$, or A_k as described in Holtzman et al. (2015). Initially, we excise objects with $3500 < T_{\text{eff}} < 6000$, with $[\alpha/\text{M}] < 0.1$ dex, or with ASPCAPFLAG set. We then train the model on the remaining objects, apply this model to the reference set (cross-calibration) and discard objects whose difference from the reference (APOGEE) value in any particular label is greater than four times the scatter in that label. This leaves 9952 objects.

The distribution of these 9952 reference objects in (LAMOST T_{eff} , LAMOST $\log g$) label space is shown in Figure 3. The black points in the background are the full LAMOST DR2 sample, with their values from the LAMOST pipeline. The overlaid colored points are the reference objects; in the left panel, they are shown with their LAMOST pipeline values, and in the right panel, they are shown with their APOGEE pipeline values. It is only the

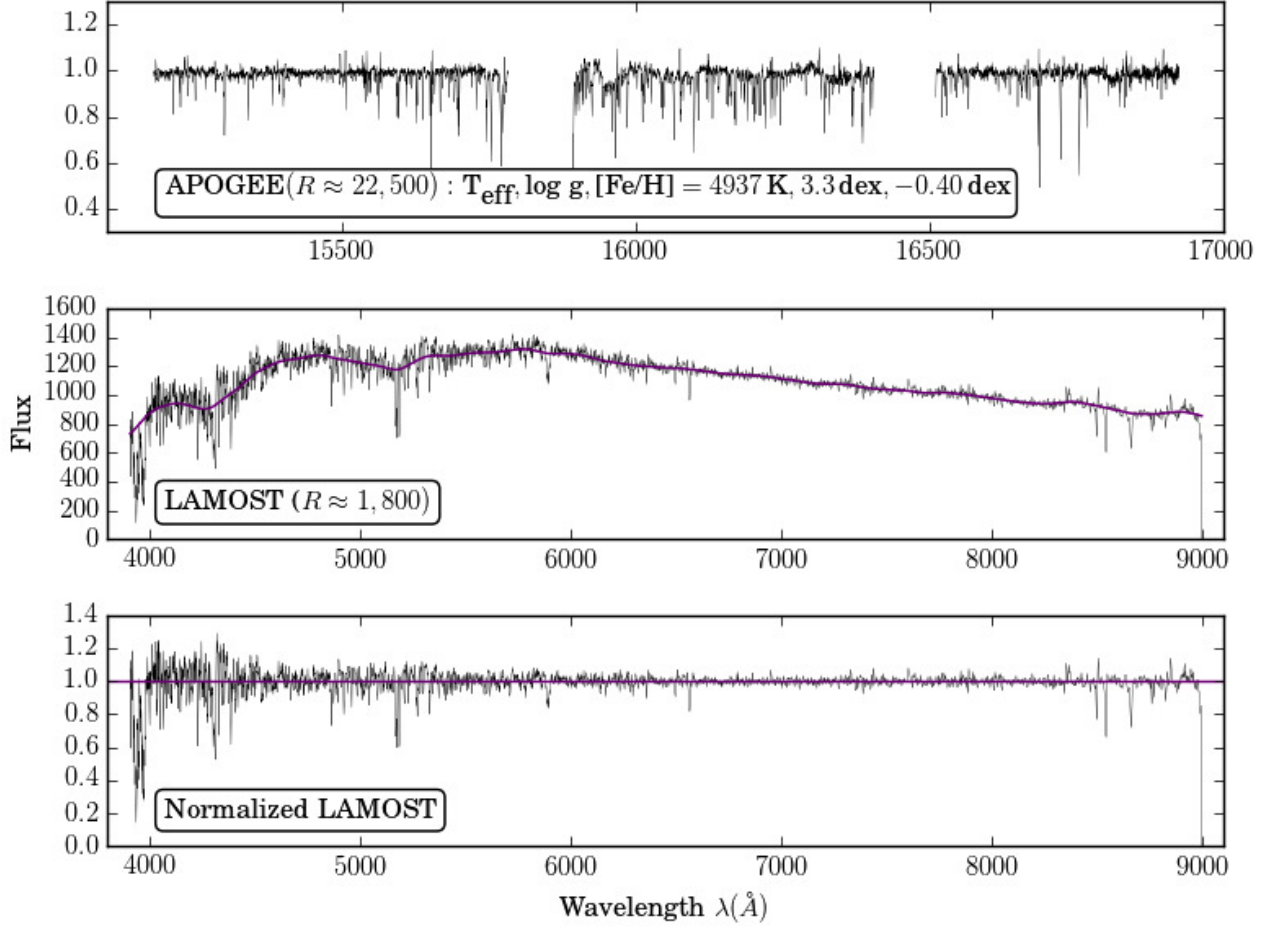


Fig. 2.— Spectra of a sample reference object (2MASS ID 2M07101078+2931576). The top panel shows the normalized APOGEE spectrum (with its basic stellar labels) and the middle panel shows the raw LAMOST spectrum overlaid with the Gaussian-smoothed version of itself. The bottom panel shows the resulting “normalized” spectrum, determined by dividing the black line by the purple line in the middle panel. *The Cannon* operates on the normalized spectrum in the bottom panel, although note that this “normalization” is different from the standard normalization used in spectral analysis. APOGEE and LAMOST spectra are qualitatively very different, in wavelength coverage and resolution.

APOGEE labels, shown as colored dots in the right panel, that are used in the training step.

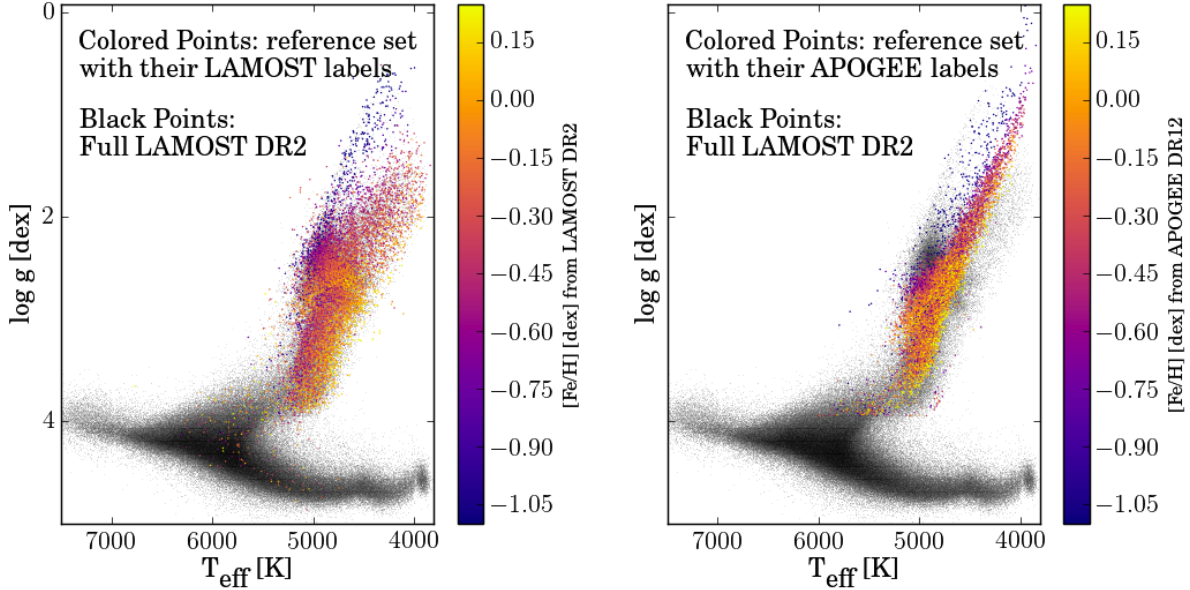


Fig. 3.— LAMOST DR2 (black points), overlaid with the reference set of 9952 objects (colored points) used to train the spectral model. These colored points are objects that have been observed by both LAMOST and APOGEE; in the left panel, they are shown with their LAMOST pipeline values, and in the right panel, they are shown with their APOGEE pipeline values. It is the values in the right panel that are used to train the spectral model.

The Cannon uses the reference objects to fit for a spectral model that characterizes the flux in each pixel of the (normalized) spectrum as a function g of the labels of the star. In general, the flux $f_{n\lambda}^B$ for object n at wavelength λ in Survey B can be written as

$$f_{n\lambda}^B = g(\ell_n^A | \theta_\lambda) + \text{noise} \quad (3)$$

where θ_λ is the set of spectral model coefficients at each wavelength λ of the Survey B spectrum and ℓ_n^A is some (possibly complicated) function of the full set of labels (from Survey A). The noise model is $\text{noise} = [s_\lambda^2 + \sigma_{n\lambda}^2] \xi_{n\lambda}$, where each $\xi_{n\lambda}$ is a Gaussian random number with zero mean and unit variance. The noise is thus a root-mean-square (rms) combination of inherent uncertainty in the spectrum from e.g. instrument effects and finite photon counts ($\sigma_{n\lambda}$) and intrinsic scatter in the model at each wavelength (s_λ). Handling uncertainties by fitting for a noise model independently at each pixel is a key feature of *The Cannon* and distinguishes it from traditional machine learning methods.

Following Ness et al. (2015) we presume that the model g can be written as a linear function of $\boldsymbol{\ell}_n$:

$$f_{n\lambda}^B = \boldsymbol{\theta}_\lambda^T \cdot \boldsymbol{\ell}_n^A + \text{noise} \quad (4)$$

corresponding to the single-pixel log likelihood function

$$\ln p(f_{n\lambda}^B | \boldsymbol{\theta}_\lambda^T, \boldsymbol{\ell}_n^A, s_\lambda^2) = -\frac{1}{2} \frac{[f_{n\lambda}^B - \boldsymbol{\theta}_\lambda^T \cdot \boldsymbol{\ell}_n^A]^2}{s_\lambda^2 + \sigma_{n\lambda}^2} - \frac{1}{2} \ln(s_\lambda^2 + \sigma_{n\lambda}^2) \quad . \quad (5)$$

For this work, once more as in Ness et al. (2015), we use a quadratic model such that $\boldsymbol{\ell}_n$ is

$$\begin{aligned} \boldsymbol{\ell}_n^A \equiv & \left[1, T_{\text{eff}}, \log g, [\text{Fe}/\text{H}], [\alpha/\text{M}], A_k, \right. \\ & T_{\text{eff}} \cdot \log g, T_{\text{eff}} \cdot [\text{Fe}/\text{H}], T_{\text{eff}} \cdot [\alpha/\text{M}], T_{\text{eff}} \cdot A_k, \log g \cdot [\text{Fe}/\text{H}], \log g \cdot [\alpha/\text{M}], \\ & \log g \cdot A_k, [\text{Fe}/\text{H}] \cdot [\alpha/\text{M}], [\text{Fe}/\text{H}] \cdot A_k, [\alpha/\text{M}] \cdot A_k, \\ & \left. T_{\text{eff}}^2, \log g^2, [\text{Fe}/\text{H}]^2, [\alpha/\text{M}]^2, A_k^2 \right]_{\text{SurveyA}} \end{aligned} \quad (6)$$

The training step thus consists of holding the labels in the label vector $\boldsymbol{\ell}_n^A$ fixed (these are the reference labels) and optimizing the log likelihood to solve for the coefficients $[\boldsymbol{\theta}_\lambda, s_\lambda^2]$ independently at every pixel. For a fixed scatter value, optimization is a pure linear-algebra operation (weighted least squares). Currently, we optimize for the scatter by stepping through a grid of scatter values.

Figure 4 shows the leading (linear) coefficient for each label as a function of wavelength, as well as the scatter as a function of wavelength. The magnitude of the leading coefficient can be thought of as the sensitivity of a particular pixel is to that particular label. Thus, Figure 4 is a way to visualize which regions of the spectrum are (as determined by *The Cannon*) important for which labels. We find that T_{eff} , $\log g$, $[\text{Fe}/\text{H}]$, and $[\alpha/\text{M}]$ all have strong sensitivity to well-known spectral features such as Mg I, Na I D, and the Ca II triplet.

Interestingly, we find that A_k has strong sensitivity not only to the Na I D doublet, but also to features that correspond to known diffuse interstellar bands (DIBs). The strongest of these DIBs are indicated by the orange lines in the lower panels of Figure 4. DIBs are absorption features that appear to arise from diffuse interstellar material; see Sarre (2006)

and Herbig (1995) for extensive reviews. Over four hundred have been detected to date, mostly at optical wavelengths, but their origin remains uncertain (Hobbs et al. 2008; Herbig 1993). DIB strength has been found to correlate well with extinction and the column density of neutral hydrogen (Friedman et al. 2011). In addition, some DIBs seem to have correlated strengths, which suggests a shared origin (McCall et al. 2010; Friedman et al. 2011). Large-scale studies of DIBs (e.g. Yuan & Liu (2012)) hold promise for learning not only about their origin but also for mapping their environment; Zasowski et al. (2015) used DIBs in APOGEE infrared spectra to find that DIB strength is linearly correlated with extinction and thus a powerful probe of the structure and properties of the ISM. It is therefore perhaps not surprising that *The Cannon* learned to associate A_k with DIB strength; features in the leading coefficients plot include well-known DIBs, e.g. at 4428 Å, 4882 Å, 5780 Å, 5797 Å, 6203 Å, 6283 Å, 6614 Å, and 8621 Å. Note that the DIBs in the Cannon model are effectively smeared across the radial velocity dispersion of the training sample.

4. *The Cannon* Test Step: Deriving New Stellar Labels from LAMOST Spectra

In the training step (see Section 3), we treated the labels ℓ_n^A as known and solved for the coefficients θ_λ of the spectral model. Now, in the test step, we take these spectral model coefficients and solve for new labels ℓ_n^B (as opposed to ℓ_n^A), based on the spectra $f_{n\lambda}^B$ for each test object n . For a model that is quadratic in the labels, like ours, this consists of non-linear optimization. We use Python’s `curve_fit` routine with seven starting points in label space, to assure convergence.

Before deriving new stellar labels for LAMOST objects, we feed the 9952 reference objects back into *The Cannon* for cross-validation. Figure 5 shows the four labels (T_{eff} , $\log g$, $[\text{Fe}/\text{H}]$ and $[\alpha/\text{M}]$) as determined by *The Cannon* directly from LAMOST spectra, plotted against the corresponding APOGEE (reference) labels, determined by ASPCAP directly from APOGEE spectra. For completeness, we show the output for extinction in the final panel (light purple). Note that, in this work, we consider extinction as a “nuisance” label: we fit for it in order to more reliably determine the four other labels, but the question of how to use *The Cannon* to reliably determine extinction values from spectra is beyond the scope of this work. The low scatter and bias in the $[\alpha/\text{M}]$ panel (bottom right) shows how well *The Cannon* transferred a *new* label to the LAMOST data set. The scatter in all four labels for the objects with high S/N LAMOST spectra is comparable to the typical uncertainties from ASPCAP: 91.5 K in T_{eff} , 0.11 in $\log g$, and around 0.05 in both $[\text{Fe}/\text{H}]$ and $[\alpha/\text{M}]$ (Holtzman et al. 2015). Note that the scatter in $[\alpha/\text{M}]$ derived from the LAMOST

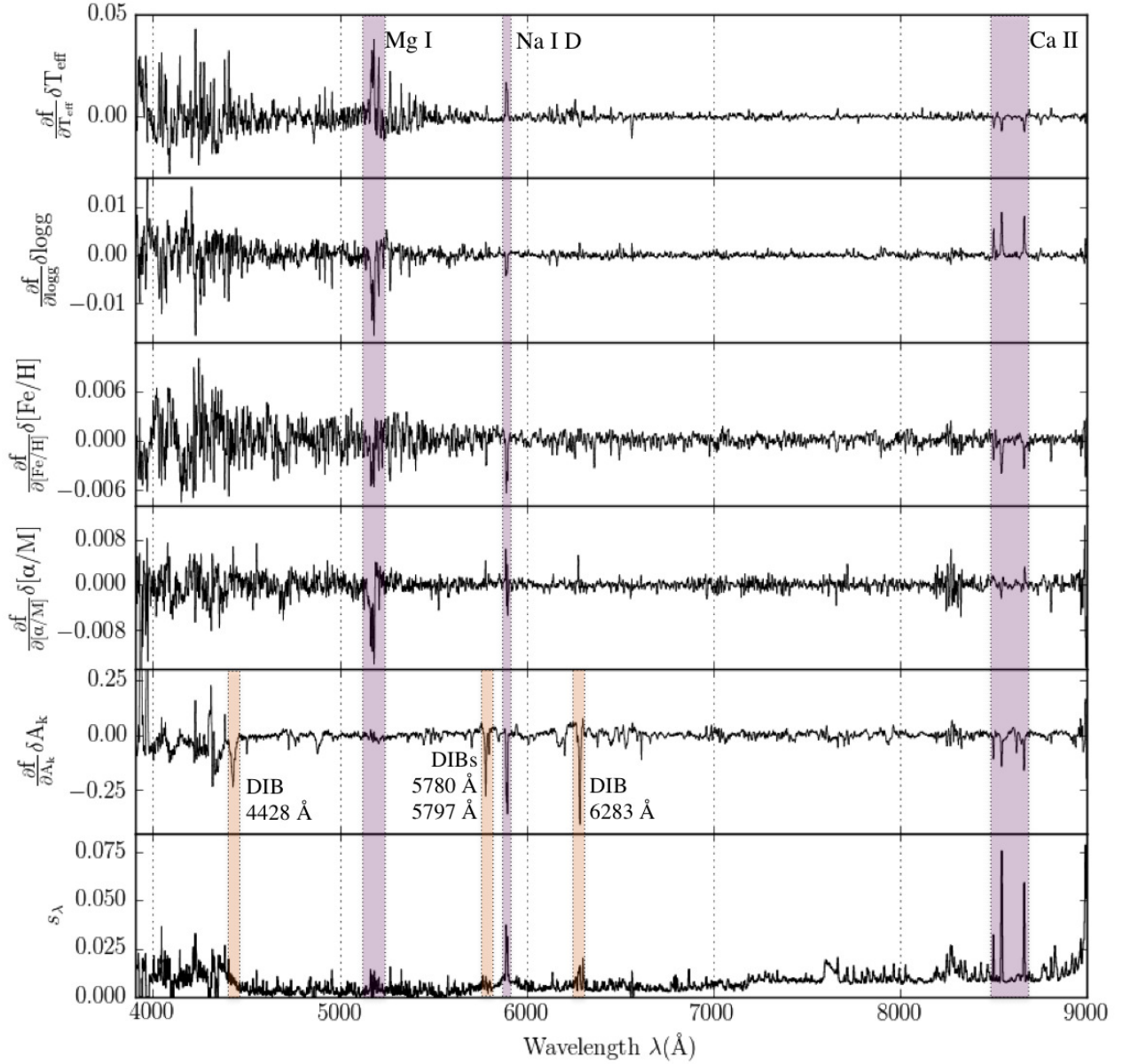


Fig. 4.— Leading (linear) coefficients and scatter from the best-fit spectral model, with prominent features labeled. These coefficients indicate how sensitive each pixel in the spectrum is to each of the labels. In the top four panels, note peaks at well-known spectral features such as the Mg I triplet around 5170 Å and the Ca II triplet around 8600 Å. In the fifth panel, note peaks at well-known diffuse interstellar bands (DIBs). The coefficients are scaled by the approximate errors in the labels (91.5 K in T_{eff} , 0.11 in $\log g$, 0.05 in $[\text{Fe}/\text{H}]$ and $[\alpha/\text{M}]$; Holtzman et al. (2015)).

spectra is very similar to the precision in $[\alpha/Fe]$ inferred indirectly for the Segue G-dwarfs by Bovy et al. (2012), based on SDSS spectra at similar resolution, wavelength coverage and S/N.

This information is represented as residuals in Figure 6; a direct comparison with Figure 1 shows a significant improvement in scatter and a dramatic reduction of systematic differences between the labels derived from LAMOST and APOGEE spectra, particularly in $\log g$ and $[Fe/H]$. The inter-survey biases in the three labels have all but vanished, demonstrating that we have successfully measured APOGEE-scale labels directly from LAMOST spectra, thus bringing the two surveys onto the same scale. Note also, that the scatter (at a given S/N) has been reduced considerably: *The Cannon* can also measure more precise labels from the low-resolution LAMOST spectra (Ness et al. 2015).

Furthermore, *The Cannon* performs more precisely at low S/N than the LAMOST pipeline, as seen in Figure 7. Here, for a S/N metric, we define “ $\sim \text{SNR}_g$.” We quantify S/N in the g-band because the leading coefficients show that decisive information comes from this regime. Furthermore, the error bar and S/N should reflect the variance of each pixel around the best-fit model; thus, the χ^2 of a model that fits well (in this case, the model from *The Cannon*) should roughly equal the number of pixels in the spectrum, 3626. Instead, the χ^2 led us to find that the errors and S/N in the spectra needed to be adjusted by a factor of three. Thus, $\sim \text{SNR}_g$ represents the S/N in the g-band, multiplied by three.

Figure 8 provides verification that the label transfer in T_{eff} and $\log g$ has led to astrophysically plausible results. It compares the $(T_{\text{eff}}, \log g)$ distribution for all reference objects using their labels from the APOGEE pipeline, from the LAMOST pipeline, and from the Cannon model for the LAMOST data. Both the morphology of the red clump and of the giant branch shows that the Cannon labels are physically much more plausible than the pipeline labels derived from the same LAMOST data.

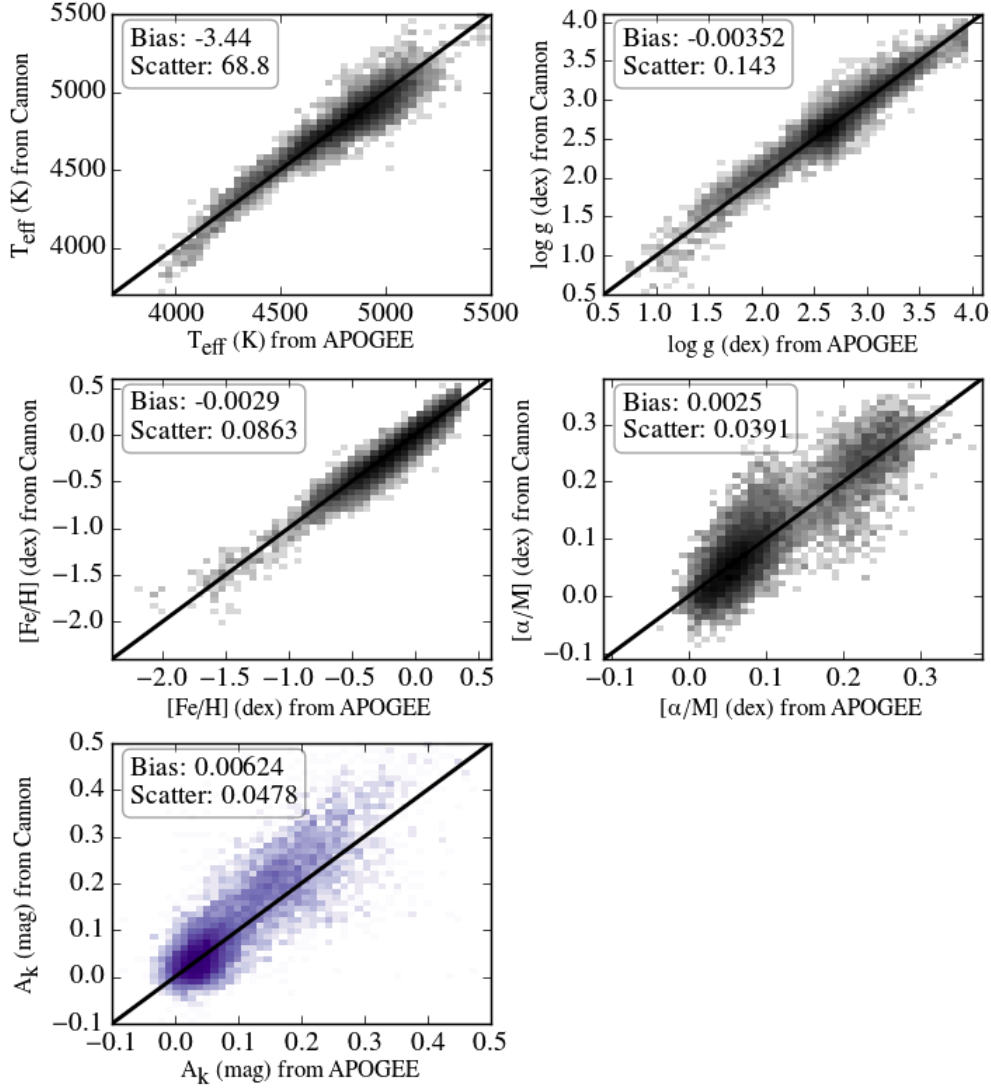


Fig. 5.— Cross-validation of *The Cannon*’s label transfer from APOGEE to LAMOST : Shown are the APOGEE labels of all reference objects compared to the labels derived from LAMOST data by *The Cannon* in the test step. Strictly speaking, this is a leave-none-out test, but we have verified that training on 80% of the reference set and testing on the remaining 20% gives consistent results. The tight one-to-one correlations in the T_{eff} , $\log g$ and $[\text{Fe}/\text{H}]$ panels simply reflect the quality of the label transfer demonstrated already in Figure 6. The bottom right panel shows how well *The Cannon* is able to transfer the *new* label $[\alpha/\text{M}]$ from APOGEE. For completeness, we include extinction as a fifth panel, but emphasize that ours is not a reliable method for inferring extinction from LAMOST spectra. The scatter and bias values represent spectra with $S/N > 50$.

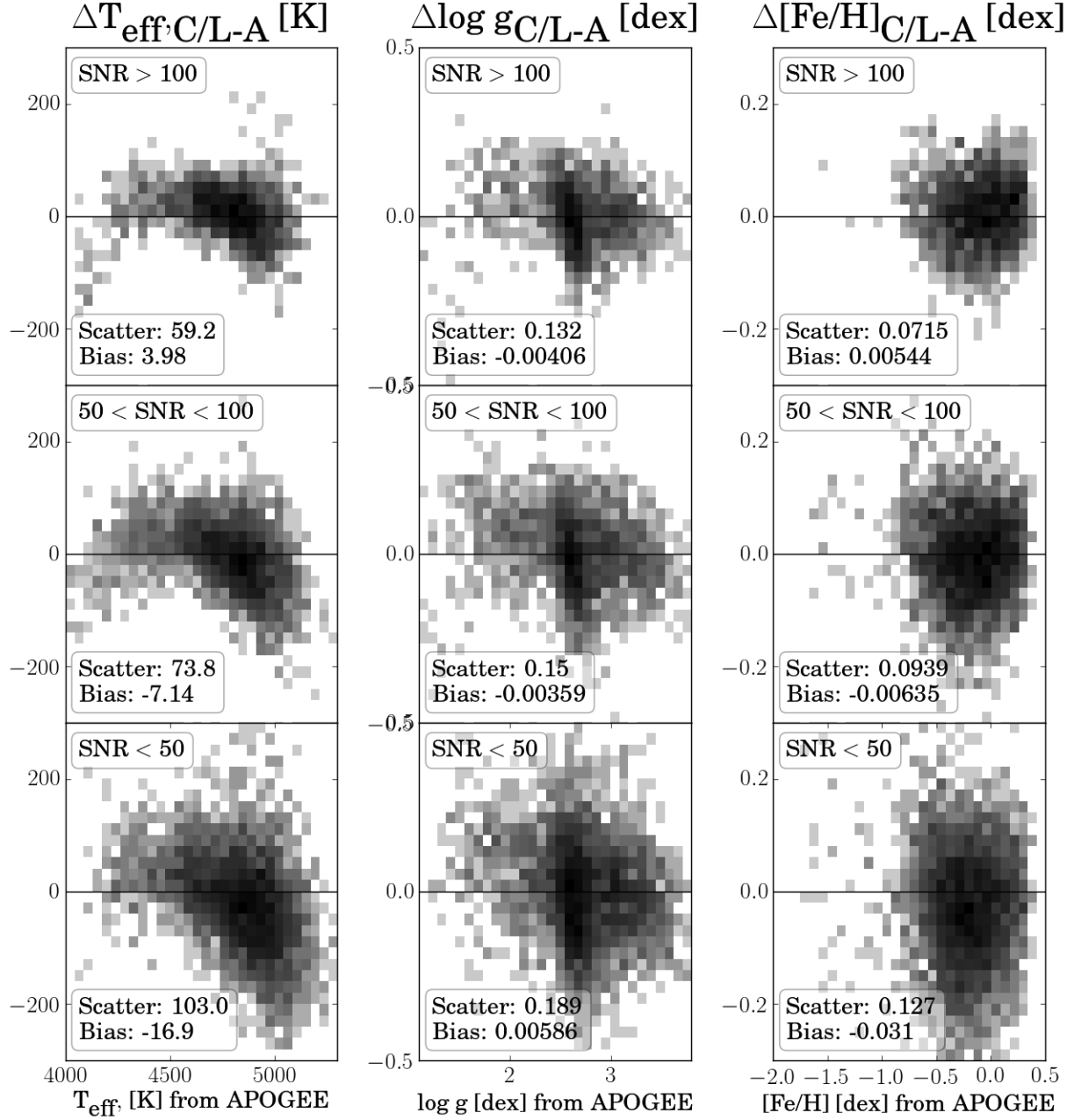


Fig. 6.— Comparison between *The Cannon* output and APOGEE reference labels : Shown here are labels for the 9952 in the reference set, objects measured in common between LAMOST and APOGEE. The systematic differences between labels determined by *The Cannon* from LAMOST spectra and by ASPCAP from APOGEE spectra have been almost completely eliminated (see (Figure 1). The Cannon values also show a substantially reduced scatter with respect to the APOGEE-labels, presumed to be ground-truth here.

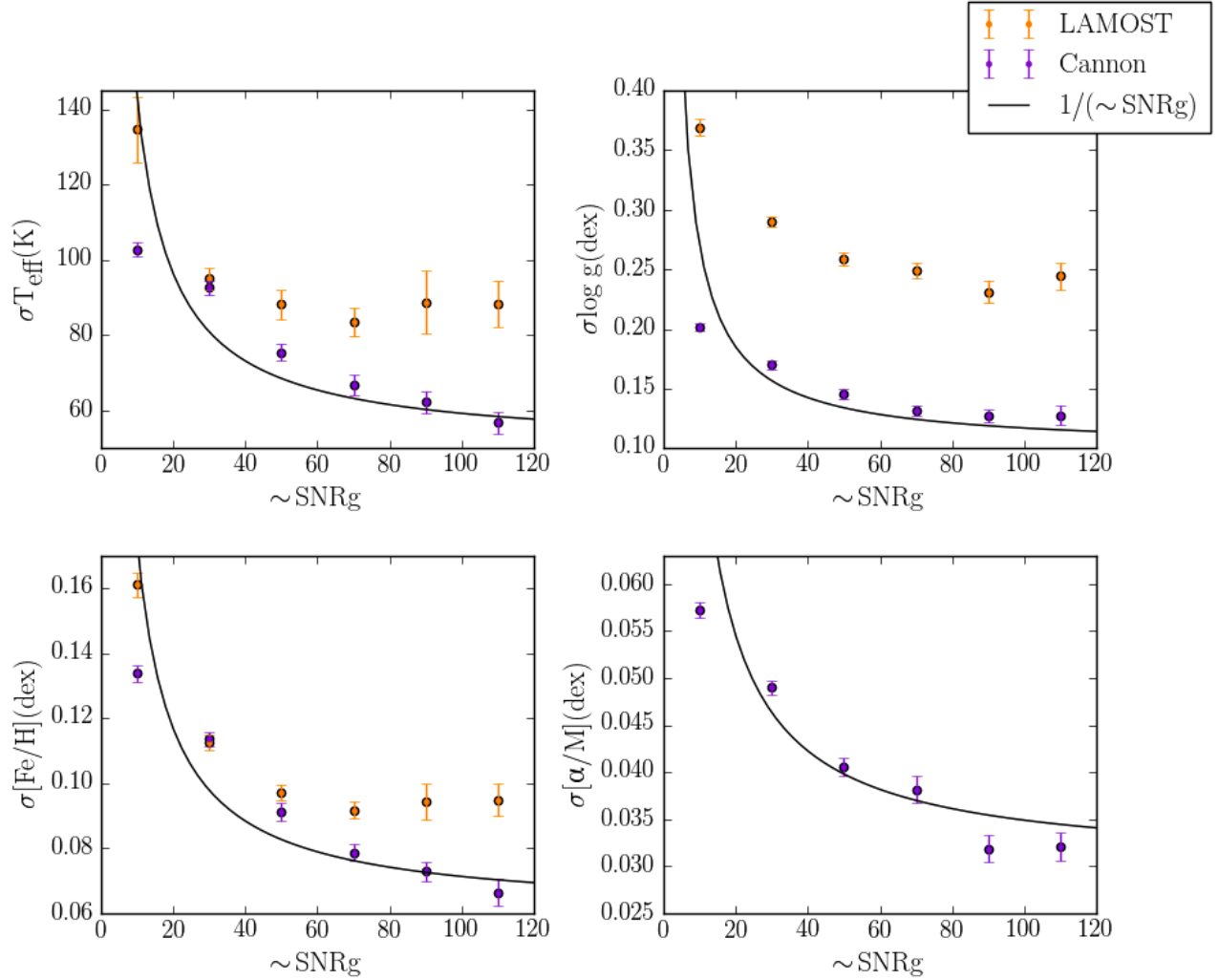


Fig. 7.— The S/N-dependence of the scatter between APOGEE DR12 labels and the corresponding labels measured from LAMOST spectra by *The Cannon* (red points) and *ULySS* (blue points). *The Cannon* represents a substantial improvement from the LAMOST pipeline in the three labels that the the APOGEE and LAMOST pipelines measure in common. The performance improvement is generally steeper than the inverse of the S/N. Note that we are using our own value for $\sim \text{SNR}_g$, which does not reflect the reported LAMOST error bar.

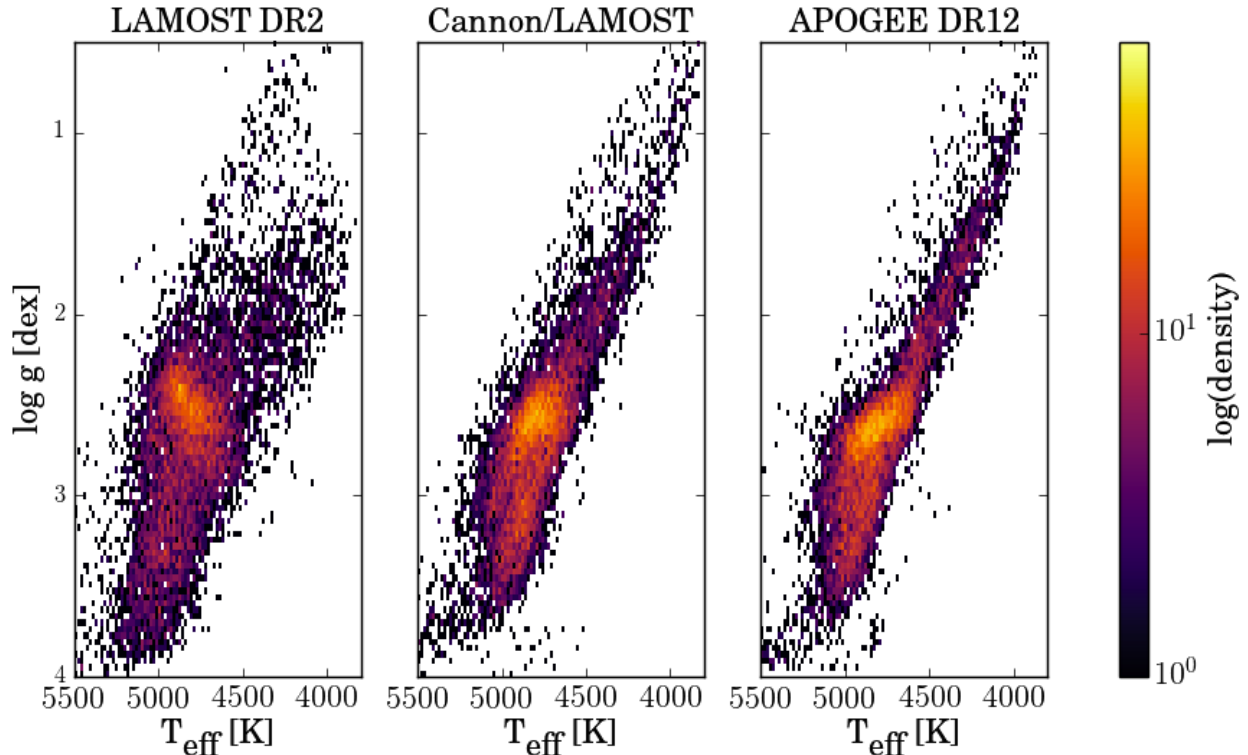


Fig. 8.— Astrophysical verification of the labels derived by *The Cannon* model for LAMOST data: the panel show the distribution of all reference objects in the $(T_{\text{eff}}, \log g)$ plane, using their LAMOST DR2 labels (left), Cannon labels from LAMOST spectra (center), and APOGEE DR12 labels (right). The distribution of Cannon labels is not only much more similar to ASPCAP’s labels, but also much more physically plausible, exhibiting a tighter red clump and a more well-defined upper giant branch.

We then apply the spectral model to DR2 objects that were *not* observed by APOGEE. *The Cannon* cannot extrapolate to regimes of $(T_{\text{eff}}, \log g, [\text{Fe}/\text{H}], [\alpha/\text{M}])$ label space that are completely different from those represented in the reference set, as shown in Ness et al. (2015). Therefore we restrict our test set to LAMOST DR2 objects that are reasonably close to the reference set in label space. To do so, we define a “label-distance” D from the reference objects in label space, exploiting here that all test objects have (initial) stellar labels estimates from the LAMOST pipeline. The label-distance of a LAMOST test object (in LAMOST label space; subscript L) and a reference object (in APOGEE label space; subscript A) is

$$D = \frac{1}{K_{T_{\text{eff}}}^2} (T_{\text{eff},L} - T_{\text{eff},A})^2 + \frac{1}{K_{\log g}^2} (\log g_L - \log g_A)^2 + \frac{1}{K_{[\text{Fe}/\text{H}]}^2} ([\text{Fe}/\text{H}]_L - [\text{Fe}/\text{H}]_A)^2, \quad (7)$$

where we have normalized by the approximate uncertainty in each label: $K_{T_{\text{eff}}} = 100$, $K_{\log g} = 0.20$, and $K_{[\text{Fe}/\text{H}]} = 0.10$. We then calculate an object’s label-distance from the reference set by taking the average of its label-distances to the ten nearest reference objects.

We use these label-distances to define the regime within which a LAMOST DR2 object was deemed a feasible test object. The label-distance cut was determined by running the test step of *The Cannon* on 3,000 random objects in LAMOST DR2. In Figure 9 we show the label-distance from the Cannon-inferred labels to the original LAMOST pipeline labels, plotted against each object’s label-distance from the reference set. Figure 9 shows a gap along the x-axis, separating the giant branch (close to the reference set) from the main sequence. Figure 10 shows 14,000 random stars in the $(T_{\text{eff}}, \log g)$ -plane (colored points), on top of the entire LAMOST DR2 sample (see Figure 3): a label-distance cut at 2.5 neatly separates the giants (to which the spectral model applies) from the main sequence stars.

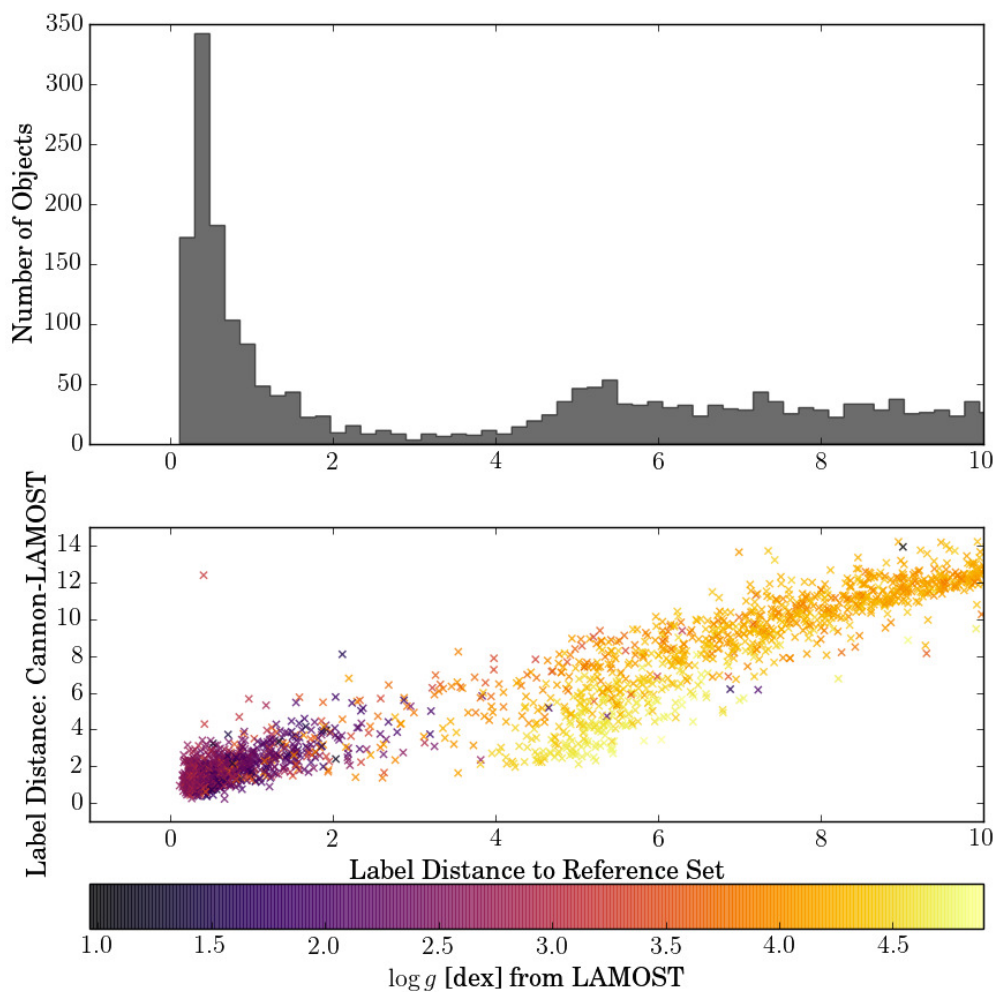


Fig. 9.— Label Distance of LAMOST Objects from Reference Set: Giant branch stars and main sequence stars in LAMOST DR2 separate out when their distance from reference label space is plotted against the distance from their LAMOST labels to their Cannon labels, which are determined by running these stars through *The Cannon* test step. We use this to inform our choice of test objects: we select those with a label distance to the reference set of less than 2.5.

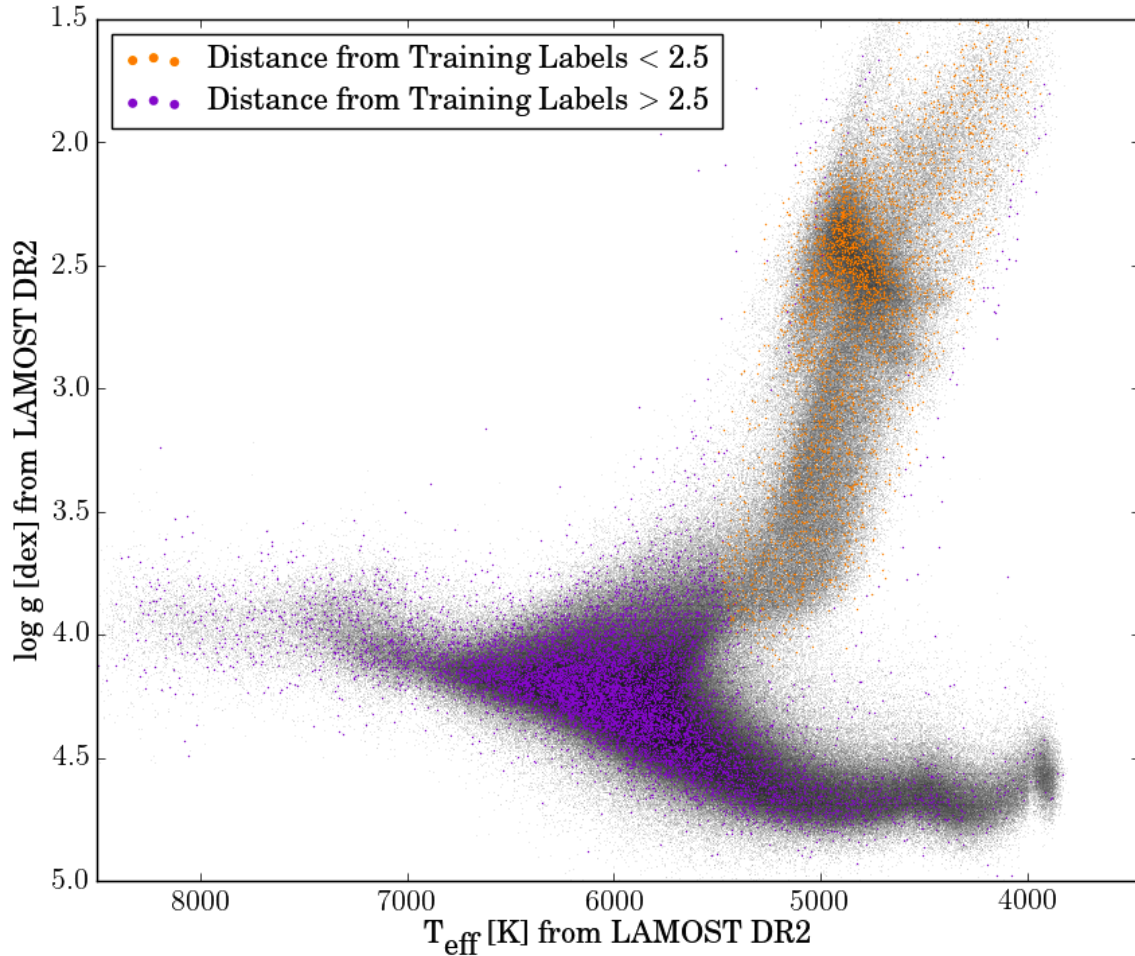


Fig. 10.— Label Distance From Reference Set: (Black) all LAMOST DR2 points in $(T_{\text{eff}}, \log g)$ space, with (Color) 14,000 objects overlaid color-coded by their distances from the reference label space. For the test step, we choose objects whose distances are less than 2.5, which corresponds to the giant branch.

We define the test set as all LAMOST DR2 objects with a label-distance from the reference set of < 2.5 . After using the spectral model to infer new labels, we excise objects for which the convergence either failed or resulted in a fit with reduced $\chi^2 > 10$ (fewer than 0.1% of the objects). This leaves 444,228 stars (giants), not including the reference set. The newly inferred labels for these objects, together with the *Cannon* labels for the reference set and their associated formal errors, are available in a table online and an excerpt is shown in Table 1. This table includes the first-ever $[\alpha/M]$ values measured from LAMOST spectra.

To estimate the errors on these labels, we need to take into account the incomplete and

sometimes sparse coverage of label space by the reference objects. *The Cannon* only returns formal (statistical) error bars, which do not take systematic sources of error (e.g. errors on the input labels, sparsity of label coverage) into account. Thus, we create 20 different spectral models by bootstrap-sampling from the set of reference objects. For each set, we run the cross-calibration as described in Figure 5. A subset of the test set has 20 different label estimates, and we adopt the standard deviation of these measurements as an approximate error bar on these new LAMOST labels. With such a large training sample with which to fit the spectral model, the values are negligible: 4.4 K for T_{eff} , 0.012 dex for $\log g$, 0.0060 dex for $[\text{Fe}/\text{H}]$, and 0.0042 dex for $[\alpha/\text{M}]$.

Table 1: Excerpt from the online table of stellar labels (T_{eff} , $\log g$, $[\text{Fe}/\text{H}]$, and $[\alpha/\text{M}]$) for 454,180 stars, inferred by *The Cannon* directly from LAMOST spectra. Column 1 is the LAMOST ID of the object, Columns 2-5 are the labels from *The Cannon*, Columns 6-9 are the formal errors on those labels from *The Cannon*, and the final column is the reduced χ^2 . Note that the reduced χ^2 values are low by a factor of ~ 3 because the random component of the errors in the LAMOST spectra is overestimated (see Section 4).

LAMOST ID	T_{eff} (K)	$\log g$ (dex)	$[\text{Fe}/\text{H}]$ (dex)	$[\alpha/\text{M}]$ (dex)	$\sigma(T_{\text{eff}})$ (K)	$\sigma(\log g)$ (dex)	$\sigma([\text{Fe}/\text{H}])$ (dex)	$\sigma([\alpha/\text{M}])$ (dex)	Red. χ^2
spec-55859-F5902_sp01-034.fits	4899	3.15	-0.597	0.207	48	0.08	0.053	0.024	0.62
spec-55859-F5902_sp01-136.fits	5279	3.08	-0.838	0.206	145	0.29	0.177	0.075	0.57
spec-55859-F5902_sp01-202.fits	4884	3.25	-0.383	0.225	36	0.06	0.040	0.016	0.82
spec-55859-F5902_sp01-207.fits	4882	3.43	-0.252	0.186	39	0.06	0.043	0.017	0.88

4.1. The $[\alpha/\text{M}]$ Map of the Milky Way from LAMOST

The full astrophysical verification and exploitation of the new set of labels for the LAMOST DR2 giants is beyond the scope of the paper. Here, we give some initial indication of what will be enabled, by showing the ($[\text{Fe}/\text{H}], [\alpha/\text{M}]$) plane (Figure 11) and the distribution of $[\alpha/\text{M}]$ in galactic latitude and longitude (Figure 12) for all LAMOST DR2 giants. This is by far the largest set of giants with the $[\alpha/\text{M}]$ abundance label. As Fig. 12 shows, the combination of the two surveys overcomes a limitation of many previous analyses of the abundance-dependent Galactic disk structure (see e.g. Rix & Bovy (2013)): most large surveys have either extensive coverage at high Galactic latitudes with sparse sampling in the Galactic plane, or vice versa. The distribution in the ($[\text{Fe}/\text{H}], [\alpha/\text{M}]$) plane looks very plausible, exhibiting the α -enhanced and the low- α sequences, and the spatial distribution beautifully exhibits the low-alpha, chemically late, young population in the mid-plane and at large radii, and the alpha-enhanced, rapidly enriched, old population in the thick disk (high latitudes) and Galactic center.

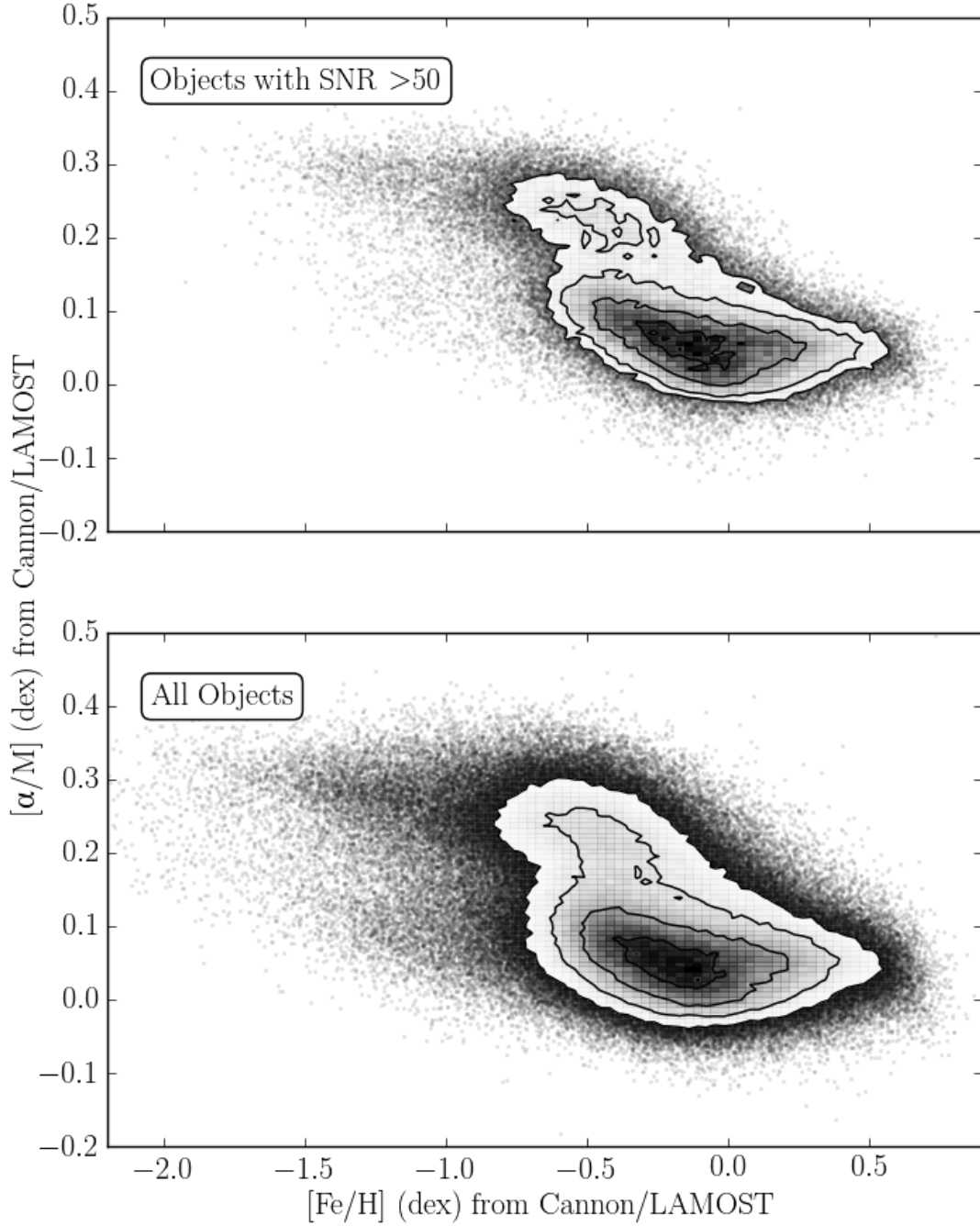


Fig. 11.— The $([\alpha/M], [Fe/H])$ plane, showing the labels determined by *The Cannon* for all 454,180 objects. The raw values are shown as grayscale points and the contours (made from logarithmic bins) are at 0.5, 1, 1.5, and 2 sigma. These are the first $[\alpha/M]$ values measured from LAMOST spectra, and by far the largest set of giants with this abundance label. Figure made using code from Dan Foreman-Mackey et al. (2014).

5. Discussion

We have demonstrated that *The Cannon* can be used to put two spectroscopic stellar surveys with very different experimental set-ups (wavelength coverage, resolution) onto the same label (stellar parameter and chemical abundance) scale by training a spectral model on the set of objects observed in common between the surveys. We used LAMOST and APOGEE as our example, and showed that we can greatly reduce the systematic differences between labels measured using the two individual survey pipelines. We can also boost the precision of the label estimates for the data set of less resolution and S/N (LAMOST in this case). By training our model to infer APOGEE-scale stellar labels directly from LAMOST spectra, we can also transfer new labels from one survey to another for: here we derived $[\alpha/M]$ from LAMOST spectra for the first time.

There are substantial benefits to using *The Cannon* for survey cross-calibration. As described in (Ness et al. 2015), *The Cannon* is very fast: for 9952 objects, on a regular computer, the training step took a few minutes and the test step for 444,228 test objects (i.e. the label determination) took a few hours. In addition, *The Cannon* requires no physical models and performs well at low S/N and low resolution: in this case, we were able to measure labels of comparable precision to APOGEE (at least, to ASPCAP’s stated precision; see Ness et al. (2015)) from LAMOST’s substantially lower resolution and lower S/N spectra (see Figure 7). Finally, because *The Cannon* fits for a set of model coefficients independently at each wavelength of the spectrum, there is a straightforward way to investigate the information content of a particular wavelength regime and determine where and how information about a particular label is encoded (see Figure 4).

This cross-calibration effort was both enabled and severely limited by the reference set: the large number of objects with reliable labels (9952) measured in common between the two surveys enabled us to fit for a spectral model, but the incomplete label coverage restricted the applicability of the model to only 454,180 out of several million LAMOST objects. To take full advantage a data-driven approach like *The Cannon*, it is essential for surveys to measure objects in common that have high-fidelity labels comprehensively spanning the label space of interest.

Clearly, *The Cannon* holds promise for bringing other overlapping surveys onto the same label scale (e.g. RAVE, SEGUE, GALAH, Gaia-ESO). Looking ahead, Gaia will provide a billion low-resolution spectra. By the time these spectra become available, over a million of these objects will have spectroscopic labels determined by much higher resolution ground-based spectra. This offers a tremendous opportunity for transferring high-quality spectral labels to low-resolution Gaia spectra, if not with the present version of *The Cannon* then with the basic underlying ideas of data-driven spectral modeling.

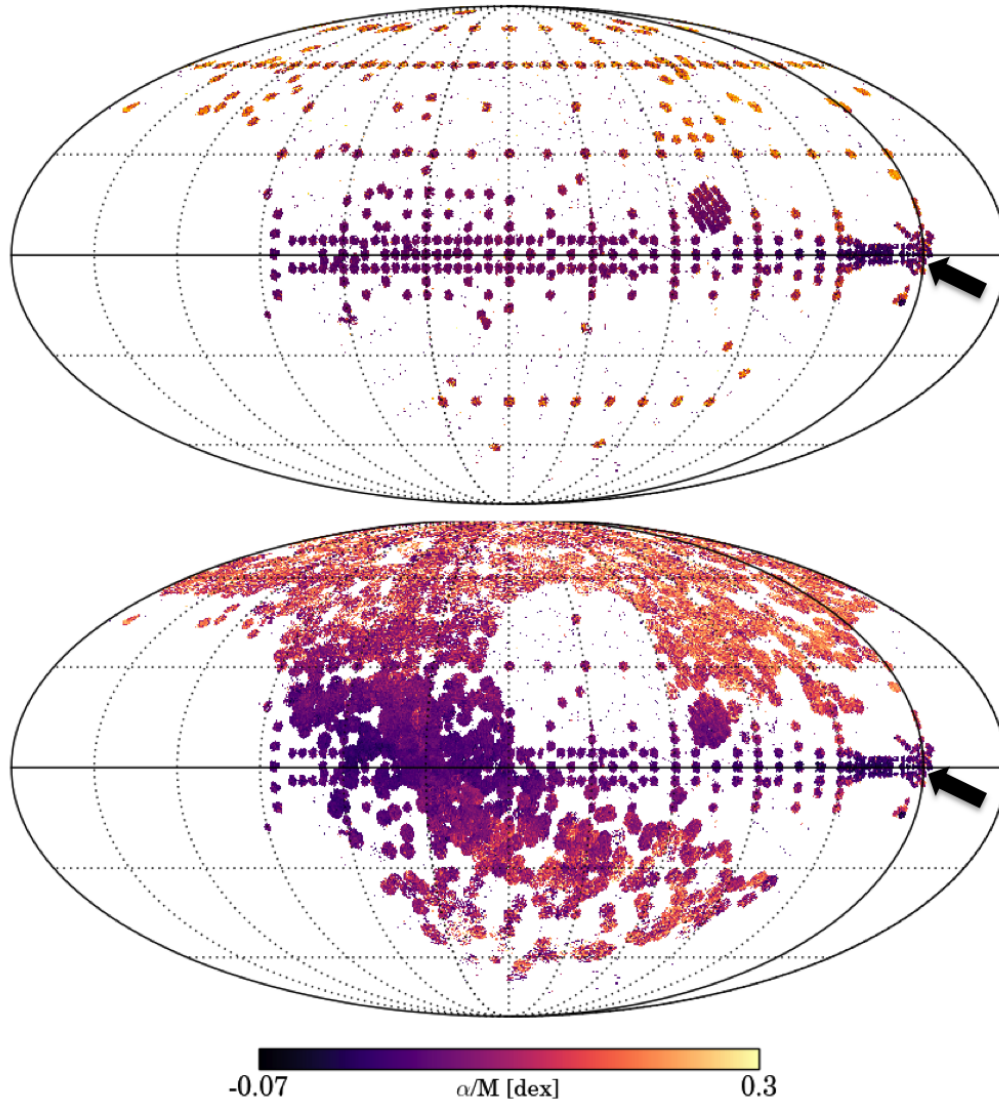


Fig. 12.— The distribution on the sky (in Galactic coordinates) of the full set of objects with consistently measured $[\alpha/M]$: the top panel shows the full APOGEE sample with $\approx 100,000$ objects, and the bottom panel shows these values combined with 454,180 $[\alpha/M]$ inferred by *The Cannon* from the LAMOST spectra. The much more extensive area coverage of the LAMOST data is immediately apparent. One can clearly see how the low- α stars, presumably a younger population from more slowly enriched gas, is concentrated towards the mid-plane. The α -enhanced stars, mostly a rapidly enriched, old population, are found in the in the thick disk and halo (at high latitudes), as well as the outer Galactic bulge; the arrow on the right denotes the Galactic center. This illustrates the promise of survey cross-calibration for stitching together a more complete stellar population picture of the Galaxy.

The code used to produce the results described in this paper was written in Python and is available online in an open-source repository.¹

It is a pleasure to thank Andy Casey (IoA Cambridge), Morgan Fouesneau (MPIA), Evan Kirby (Caltech), and Branimir Sesar (MPIA) for valuable discussions and assistance. AYQH is grateful to the community at the MPIA for their support and hospitality during the period in which most of this work was performed.

AYQH was supported by a Fulbright grant through the German-American Fulbright Commission and a National Science Foundation Graduate Research Fellowship under Grant No. DGE1144469. MKN and HWR have received funding for this research from the European Research Council under the European Union’s Seventh Framework Programme (FP 7) ERC Grant Agreement n. [321035]. DWH was partially supported by the NSF (grant IIS-1124794), NASA (grant NNX08AJ48G), and the Moore-Sloan Data Science Environment at NYU. CL acknowledges the Strategic Priority Research Program “The Emergence of Cosmological Structures” of the Chinese Academy of Sciences, Grant No. XDB09000000, the National Key Basic Research Program of China 2014CB845700, and the National Natural Science Foundation of China (NSFC) grants No. 11373032 and 11333003.

Guoshoujing Telescope (the Large Sky Area Multi-Object Fiber Spectroscopic Telescope LAMOST) is a National Major Scientific Project built by the Chinese Academy of Sciences. Funding for the project has been provided by the National Development and Reform Commission. LAMOST is operated and managed by the National Astronomical Observatories, Chinese Academy of Sciences.

Funding for the Sloan Digital Sky Survey IV has been provided by the Alfred P. Sloan Foundation, the U.S. Department of Energy Office of Science, and the Participating Institutions. SDSS-IV acknowledges support and resources from the Center for High-Performance Computing at the University of Utah. The SDSS web site is www.sdss.org.

SDSS-IV is managed by the Astrophysical Research Consortium for the Participating Institutions of the SDSS Collaboration including the Brazilian Participation Group, the Carnegie Institution for Science, Carnegie Mellon University, the Chilean Participation Group, the French Participation Group, Harvard-Smithsonian Center for Astrophysics, Instituto de Astrofísica de Canarias, The Johns Hopkins University, Kavli Institute for the Physics and Mathematics of the Universe (IPMU) / University of Tokyo, Lawrence Berkeley National Laboratory, Leibniz Institut für Astrophysik Potsdam (AIP), Max-Planck-Institut

¹www.github.com/annayqho/TheCannon

für Astronomie (MPIA Heidelberg), Max-Planck-Institut für Astrophysik (MPA Garching), Max-Planck-Institut für Extraterrestrische Physik (MPE), National Astronomical Observatory of China, New Mexico State University, New York University, University of Notre Dame, Observatório Nacional / MCTI, The Ohio State University, Pennsylvania State University, Shanghai Astronomical Observatory, United Kingdom Participation Group, Universidad Nacional Autónoma de México, University of Arizona, University of Colorado Boulder, University of Oxford, University of Portsmouth, University of Utah, University of Virginia, University of Washington, University of Wisconsin, Vanderbilt University, and Yale University.

Facilities: Sloan(APOGEE spectrograph), LAMOST

REFERENCES

- Alam, S., Albareti, F. D., Allende Prieto, C., et al. 2015, *ApJS*, 219, 12
- Bovy, J., Rix, H.-W., Hogg, D. W., et al. 2012, *ApJ*, 755, 115
- Chen, Y. Q., Zhao, G., Liu, C., et al. 2015, arXiv:1506.00771
- De Silva, G. M., Freeman, K. C., Bland-Hawthorn, J., et al. 2015, *MNRAS*, 449, 2604
- Eisenstein, D. J., Weinberg, D. H., Agol, E., et al. 2011, *AJ*, 142, 72
- Foreman-Mackey, D., et al. triangle.py v0.1.1. Zenodo. 10.5281/zenodo.11020
- Friedman, S. D., York, D. G., McCall, B. J., et al. 2011, *ApJ*, 727, 33
- García Pérez, A. E., Allende Prieto, C., Holtzman, J. A., et al. 2015, arXiv:1510.07635
- Gilmore, G., Randich, S., Asplund, M., Binney, J., Bonifacio, P., Drew, J., Feltzing, S., Ferguson, A., Jeffries, R., Micela, G., Negueruela, I., Prusti, T., Rix, H.-W., Vallenari, A., Alfaro, E., Allende-Prieto, C., Babusiaux, C., Bensby, T., Blomme, R., Bragaglia, A., Flaccomio, E., François, P., Irwin, M., Koposov, S., Korn, A., Lanzafame, A., Pancino, E., Paunzen, E., Recio-Blanco, A., Sacco, G., Smiljanic, R., Van Eck, S., & Walton, N. 2012, *The Messenger*, 147, 25
- Gunn, J. E., Siegmund, W. A., Mannery, E. J., et al. 2006, *AJ*, 131, 2332
- Herbig, G. H. 1993, *ApJ*, 407, 142
- Herbig, G. H. 1995, *ARA&A*, 33, 19

- Hobbs, L. M., York, D. G., Snow, T. P., et al. 2008, *ApJ*, 680, 1256
- Holtzman, J. A., Shetrone, M., Johnson, J. A., et al. 2015, arXiv:1501.04110
- Kordopatis, G., Gilmore, G., Steinmetz, M., et al. 2013, *AJ*, 146, 134
- Liu, C., Deng, L.-C., Carlin, J. L., et al. 2014, *ApJ*, 790, 110
- Liu, C., Fang, M., Wu, Y., et al. 2015, *ApJ*, 807, 4
- Luo, A.L., Bai, Z. R., et al. 2015, *RAA*, in press
- Majewski, S. R., Schiavon, R. P., Allende Prieto, C., et al. 2015, in preparation
- McCall, B. J., Drosback, M. M., Thorburn, J. A., et al. 2010, *ApJ*, 708, 1628
- Mészáros, S., Holtzman, J., García Pérez, A. E., et al. 2013, *AJ*, 146, 133
- Ness, M., Hogg, D. W., Rix, H.-W., Ho, A. Y. Q., & Zasowski, G. 2015, *ApJ*, 808, 16
- Ness, M., Hogg, D. W., Rix, H., et al. 2016, arXiv:1511.08204
- Rix, H.-W., & Bovy, J. 2013, *A&A Rev.*, 21, 61
- Sarre, P. J. 2006, *Journal of Molecular Spectroscopy*, 238, 1
- Smiljanic, R., Korn, A. J., Bergemann, M., et al. 2014, *A&A*, 570, A122
- Wan, J.-C., Liu, C., Deng, L.-C., et al. 2015, *Research in Astronomy and Astrophysics*, 15, 1166
- Wilson, J. C., Hearty, F., Skrutskie, M. F., et al. 2010, *Proc. SPIE*, 7735, 77351C
- Wu, Y., Luo, A.-L., Li, H.-N., et al. 2011, *Research in Astronomy and Astrophysics*, 11, 924
- Yanny, B., Rockosi, C., Newberg, H. J., et al. 2009, *AJ*, 137, 4377-4399
- Yuan, H. B., & Liu, X. W. 2012, *MNRAS*, 425, 1763
- Zasowski, G., Ménard, B., Bizyaev, D., et al. 2015, *ApJ*, 798, 35
- Zhao, G., Zhao, Y.-H., Chu, Y.-Q., Jing, Y.-P., & Deng, L.-C. 2012, *Research in Astronomy and Astrophysics*, 12, 723